Study of $\psi(3686) \to \Lambda\bar{\Lambda}\omega$

M. Ablikim,[1] M. N. Achasov,[10,b] P. Adlarson,[68] M. Albrecht,[4] R. Aliberti,[28] A. Amoroso,[67a,67c] M. R. An,[32] Q. An,[64,50] X. H. Bai,[58] Y. Bai,[49] O. Bakina,[29] R. Baldini Ferroli,[23a] I. Balossino,[24a] Y. Ban,[39,h] V. Batozskaya,[1,37] D. Becker,[28] K. Begzsuren,[26] N. Berger,[28] M. Bertani,[23a] D. Bettoni,[24a] F. Bianchi,[67a,67c] J. Bloms,[61] A. Bortone,[67a,67c] I. Boyko,[29] R. A. Briere,[5] A. Brueggemann,[61] H. Cai,[69] X. Cai,[1,50] A. Calcaterra,[23a] G. F. Cao,[1,55] N. Cao,[1,55] S. A. Cetin,[54a] J. F. Chang,[1,50] W. L. Chang,[1,55] G. Chelkov,[29,a] C. Chen,[36] G. Chen,[1] H. S. Chen,[1,55] M. L. Chen,[1,50] S. J. Chen,[35] T. Chen,[1] X. R. Chen,[25,55] X. T. Chen,[1] Y. B. Chen,[1,50] Z. J. Chen,[20,i] W. S. Cheng,[67c] X. Chu,[36] G. Cibinetto,[24a] F. Cossio,[67c] J. J. Cui,[42] H. L. Dai,[1,50] J. P. Dai,[71] A. Dbeyssi,[14] R. E. de Boer,[4] D. Dedovich,[29] Z. Y. Deng,[1] A. Denig,[28] I. Denysenko,[29] M. Destefanis,[67a,67c] F. De Mori,[67a,67c] Y. Ding,[33] J. Dong,[1,50] L. Y. Dong,[1,55] M. Y. Dong,[1,50,55] X. Dong,[69] S. X. Du,[73] P. Egorov,[29,a] Y. L. Fan,[69] J. Fang,[1,50] S. S. Fang,[1,55] W. X. Fang,[1] Y. Fang,[1] R. Farinelli,[24a] L. Fava,[67b,67c] F. Feldbauer,[4] G. Felici,[23a] C. Q. Feng,[64,50] J. H. Feng,[51] K. Fischer,[62] M. Fritsch,[4] C. Fritzsch,[61] C. D. Fu,[1] H. Gao,[55] Y. N. Gao,[39,h] Yang Gao,[64,50] S. Garbolino,[67c] I. Garzia,[24a,24b] P. T. Ge,[69] C. Geng,[51] E. M. Gersabeck,[59] A. Gilman,[62] K. Goetzen,[11] L. Gong,[33] W. X. Gong,[1,50] W. Gradl,[28] M. Greco,[67a,67c] M. H. Gu,[1,50] C. Y. Guan,[1,55] A. Q. Guo,[25,55] L. B. Guo,[34] R. P. Guo,[41] Y. P. Guo,[9,g] A. Guskov,[29,a] T. T. Han,[42] W. Y. Han,[32] X. Q. Hao,[15] F. A. Harris,[57] K. K. He,[47] K. L. He,[1,55] F. H. Heinsius,[4] C. H. Heinz,[28] Y. K. Heng,[1,50,55] C. Herold,[52] M. Himmelreich,[11,e] T. Holtmann,[4] G. Y. Hou,[1,55] Y. R. Hou,[55] Z. L. Hou,[1] H. M. Hu,[1,55] J. F. Hu,[48,j] T. Hu,[1,50,55] Y. Hu,[1] G. S. Huang,[64,50] K. X. Huang,[51] L. Q. Huang,[65] L. Q. Huang,[25,55] X. T. Huang,[42] Y. P. Huang,[1] Z. Huang,[39,h] T. Hussain,[66] N. Hüsken,[22,28] W. Imoehl,[22] M. Irshad,[64,50] J. Jackson,[22] S. Jaeger,[4] S. Janchiv,[26] Q. Ji,[1] Q. P. Ji,[15] X. B. Ji,[1,55] X. L. Ji,[1,50] Y. Y. Ji,[42] Z. K. Jia,[64,50] H. B. Jiang,[42] S. S. Jiang,[32] X. S. Jiang,[1,50,55] Y. Jiang,[55] J. B. Jiao,[42] Z. Jiao,[18] S. Jin,[35] Y. Jin,[58] M. Q. Jing,[1,55] T. Johansson,[68] N. Kalantar-Nayestanaki,[56] X. S. Kang,[33] R. Kappert,[56] M. Kavatsyuk,[56] B. C. Ke,[73] I. K. Keshk,[4] A. Khoukaz,[61] P. Kiese,[28] R. Kiuchi,[1] R. Kliemt,[11] L. Koch,[30] O. B. Kolcu,[54a] B. Kopf,[4] M. Kuemmel,[4] M. Kuessner,[4] A. Kupsc,[37,68] W. Kühn,[30] J. J. Lane,[59] J. S. Lange,[30] P. Larin,[14] A. Lavania,[21] L. Lavezzi,[67a,67c] Z. H. Lei,[64,50] H. Leithoff,[28] M. Lellmann,[28] T. Lenz,[28] C. Li,[36] C. Li,[40] C. H. Li,[32] Cheng Li,[64,50] D. M. Li,[73] F. Li,[1,50] G. Li,[1] H. Li,[44] H. Li,[64,50] H. B. Li,[1,55] H. J. Li,[15] H. N. Li,[48,j] J. Q. Li,[4] J. S. Li,[51] J. W. Li,[42] Ke Li,[1] L. J. Li,[1] L. K. Li,[1] Lei Li,[3] M. H. Li,[36] P. R. Li,[31,k,l] S. X. Li,[9] S. Y. Li,[53] T. Li,[42] W. D. Li,[1,55] W. G. Li,[1] X. H. Li,[64,50] X. L. Li,[42] Xiaoyu Li,[1,55] Z. Y. Li,[51] H. Liang,[1,55] H. Liang,[64,50] H. Liang,[27] Y. F. Liang,[46] Y. T. Liang,[25,55] G. R. Liao,[12] L. Z. Liao,[42] J. Libby,[21] A. Limphirat,[52] C. X. Lin,[51] D. X. Lin,[25,55] T. Lin,[1] B. J. Liu,[1] C. X. Liu,[1] D. Liu,[14,64] F. H. Liu,[45] Fang Liu,[1] Feng Liu,[6] G. M. Liu,[48,j] H. Liu,[31,k,l] H. M. Liu,[1,55] Huanhuan Liu,[1] Huihui Liu,[16] J. B. Liu,[64,50] J. L. Liu,[65] J. Y. Liu,[1,55] K. Liu,[1] K. Y. Liu,[33] Ke Liu,[17] L. Liu,[64,50] M. H. Liu,[9,g] P. L. Liu,[1] Q. Liu,[55] S. B. Liu,[64,50] T. Liu,[9,g] W. K. Liu,[36] W. M. Liu,[64,50] X. Liu,[31,k,l] Y. Liu,[31,k,l] Y. B. Liu,[36] Z. A. Liu,[1,50,55] Z. Q. Liu,[42] X. C. Lou,[1,50,55] F. X. Lu,[51] H. J. Lu,[18] J. G. Lu,[1,50] X. L. Lu,[1] Y. Lu,[1] Y. P. Lu,[1,50] Z. H. Lu,[1] C. L. Luo,[34] M. X. Luo,[72] T. Luo,[9,g] X. L. Luo,[1,50] X. R. Lyu,[55] Y. F. Lyu,[36] F. C. Ma,[33] H. L. Ma,[1] L. L. Ma,[42] M. M. Ma,[1,55] Q. M. Ma,[1] R. Q. Ma,[1,55] R. T. Ma,[55] X. Y. Ma,[1,50] Y. Ma,[39,h] F. E. Maas,[14] M. Maggiora,[67a,67c] S. Maldaner,[4] S. Malde,[62] Q. A. Malik,[66] A. Mangoni,[23b] Y. J. Mao,[39,h] Z. P. Mao,[1] S. Marcello,[67a,67c] Z. X. Meng,[58] J. G. Messchendorp,[56,d] G. Mezzadri,[24a] H. Miao,[1] T. J. Min,[35] R. E. Mitchell,[22] X. H. Mo,[1,50,55] N. Yu. Muchnoi,[10,b] H. Muramatsu,[60] Y. Nefedov,[29] F. Nerling,[11,e] I. B. Nikolaev,[10,b] Z. Ning,[1,50] S. Nisar,[8,m] Y. Niu,[42] S. L. Olsen,[55] Q. Ouyang,[1,50,55] S. Pacetti,[23b,23c] X. Pan,[9,g] Y. Pan,[59] A. Pathak,[27] M. Pelizaeus,[4] H. P. Peng,[64,50] K. Peters,[11,e] J. Pettersson,[68] J. L. Ping,[34] R. G. Ping,[1,55] S. Plura,[28] S. Pogodin,[29] R. Poling,[60] V. Prasad,[64,50] F. Z. Qi,[1] H. Qi,[64,50] H. R. Qi,[53] M. Qi,[35] T. Y. Qi,[9,g] S. Qian,[1,50] W. B. Qian,[55] Z. Qian,[51] C. F. Qiao,[55] J. J. Qin,[65] L. Q. Qin,[12] X. P. Qin,[9,g] X. S. Qin,[42] Z. H. Qin,[1,50] J. F. Qiu,[1] S. Q. Qu,[53] K. H. Rashid,[66] C. F. Redmer,[28] K. J. Ren,[32] A. Rivetti,[67c] V. Rodin,[56] M. Rolo,[67c] G. Rong,[1,55] Ch. Rosner,[14] S. N. Ruan,[36] H. S. Sang,[64] A. Sarantsev,[29,c] Y. Schelhaas,[28] C. Schnier,[4] K. Schoenning,[68] M. Scodeggio,[24a,24b] K. Y. Shan,[9,g] W. Shan,[19] X. Y. Shan,[64,50] J. F. Shangguan,[47] L. G. Shao,[1,55] M. Shao,[64,50] C. P. Shen,[9,g] H. F. Shen,[1,55] X. Y. Shen,[1,55] B.-A. Shi,[55] H. C. Shi,[64,50] J. Y. Shi,[1] R. S. Shi,[1,55] X. Shi,[1,50] X. D. Shi,[64,50] J. J. Song,[15] W. M. Song,[27,1] Y. X. Song,[39,h] S. Sosio,[67a,67c] S. Spataro,[67a,67c] F. Stieler,[28] K. X. Su,[69] P. P. Su,[47] Y.-J. Su,[55] G. X. Sun,[1] H. Sun,[55] H. K. Sun,[1] J. F. Sun,[15] L. Sun,[69] S. S. Sun,[1,55] T. Sun,[1,55] W. Y. Sun,[27] X. Sun,[20,i] Y. J. Sun,[64,50] Y. Z. Sun,[1] Z. T. Sun,[42] Y. H. Tan,[69] Y. X. Tan,[64,50] C. J. Tang,[46] G. Y. Tang,[1] J. Tang,[51] L. Y. Tao,[65] Q. T. Tao,[20,i] J. X. Teng,[64,50] V. Thoren,[68] W. H. Tian,[44] Y. Tian,[25,55] I. Uman,[54b] B. Wang,[1] B. L. Wang,[55] D. Y. Wang,[39,h] F. Wang,[65] H. J. Wang,[31,k,l] H. P. Wang,[1,55] K. Wang,[1,50] L. L. Wang,[1] M. Wang,[42] M. Z. Wang,[39,h] Meng Wang,[1,55] S. Wang,[9,g] T. Wang,[9,g] T. J. Wang,[36] W. Wang,[51] W. H. Wang,[69] W. P. Wang,[64,50] X. Wang,[39,h] X. F. Wang,[31,k,l] X. L. Wang,[9,g] Y. D. Wang,[38] Y. F. Wang,[1,50,55] Y. H. Wang,[40] Y. Q. Wang,[1] Ying Wang,[51] Z. Wang,[1,50] Z. Y. Wang,[1,55] Ziyi Wang,[55] D. H. Wei,[12] F. Weidner,[61] S. P. Wen,[1] D. J. White,[59] U. Wiedner,[4] G. Wilkinson,[62] M. Wolke,[68] L. Wollenberg,[4] J. F. Wu,[1,55] L. H. Wu,[1] L. J. Wu,[1,55] X. Wu,[9,g] X. H. Wu,[27] Y. Wu,[64] Z. Wu,[1,50] L. Xia,[64,50] T. Xiang,[39,h] D. Xiao,[31,k,l] H. Xiao,[9,g] S. Y. Xiao,[1] Y. L. Xiao,[9,g] Z. J. Xiao,[34] X. H. Xie,[39,h] Y. Xie,[42] Y. G. Xie,[1,50] Y. H. Xie,[6] Z. P. Xie,[64,50] T. Y. Xing,[1,55] C. F. Xu,[1] C. J. Xu,[51] G. F. Xu,[1] Q. J. Xu,[13] S. Y. Xu,[63] X. P. Xu,[47] Y. C. Xu,[55] F. Yan,[9,g] L. Yan,[9,g] W. B. Yan,[64,50]

W. C. Yan,[73] H. J. Yang,[43,f] H. L. Yang,[27] H. X. Yang,[1] L. Yang,[44] S. L. Yang,[55] Tao Yang,[1] Y. X. Yang,[1,55] Yifan Yang,[1,55] M. Ye,[1,50] M. H. Ye,[7] J. H. Yin,[1] Z. Y. You,[51] B. X. Yu,[1,50,55] C. X. Yu,[36] G. Yu,[1,55] T. Yu,[65] C. Z. Yuan,[1,55] L. Yuan,[2] S. C. Yuan,[1] X. Q. Yuan,[1] Y. Yuan,[1,55] Z. Y. Yuan,[51] C. X. Yue,[32] A. A. Zafar,[66] F. R. Zeng,[42] X. Zeng,[6] Y. Zeng,[20,i] Y. H. Zhan,[51] A. Q. Zhang,[1] B. L. Zhang,[1] B. X. Zhang,[1] D. H. Zhang,[36] G. Y. Zhang,[15] H. Zhang,[64] H. H. Zhang,[51] H. H. Zhang,[27] H. Y. Zhang,[1,50] J. L. Zhang,[70] J. Q. Zhang,[34] J. W. Zhang,[1,50,55] J. X. Zhang,[31,k,l] J. Y. Zhang,[1] J. Z. Zhang,[1,55] Jianyu Zhang,[1,55] Jiawei Zhang,[1,55] L. M. Zhang,[53] L. Q. Zhang,[51] Lei Zhang,[35] P. Zhang,[1] Q. Y. Zhang,[32,73] Shulei Zhang,[20,i] X. D. Zhang,[38] X. M. Zhang,[1] X. Y. Zhang,[42] X. Y. Zhang,[47] Y. Zhang,[62] Y. T. Zhang,[73] Y. H. Zhang,[1,50] Yan Zhang,[64,50] Yao Zhang,[1] Z. H. Zhang,[1] Z. Y. Zhang,[36] Z. Y. Zhang,[69] G. Zhao,[1] J. Zhao,[32] J. Y. Zhao,[1,55] J. Z. Zhao,[1,50] Lei Zhao,[64,50] Ling Zhao,[1] M. G. Zhao,[36] Q. Zhao,[1] S. J. Zhao,[73] Y. B. Zhao,[1,50] Y. X. Zhao,[25,55] Z. G. Zhao,[64,50] A. Zhemchugov,[29,a] B. Zheng,[65] J. P. Zheng,[1,50] Y. H. Zheng,[55] B. Zhong,[34] C. Zhong,[65] X. Zhong,[51] H. Zhou,[42] L. P. Zhou,[1,55] X. Zhou,[69] X. K. Zhou,[55] X. R. Zhou,[64,50] X. Y. Zhou,[32] Y. Z. Zhou,[9,g] J. Zhu,[36] K. Zhu,[1] K. J. Zhu,[1,50,55] L. X. Zhu,[55] S. H. Zhu,[63] T. J. Zhu,[70] W. J. Zhu,[9,g] Y. C. Zhu,[64,50] Z. A. Zhu,[1,55] B. S. Zou,[1] and J. H. Zou[1]

(BESIII Collaboration)

[1]*Institute of High Energy Physics, Beijing 100049, People's Republic of China*
[2]*Beihang University, Beijing 100191, People's Republic of China*
[3]*Beijing Institute of Petrochemical Technology, Beijing 102617, People's Republic of China*
[4]*Bochum Ruhr-University, D-44780 Bochum, Germany*
[5]*Carnegie Mellon University, Pittsburgh, Pennsylvania 15213, USA*
[6]*Central China Normal University, Wuhan 430079, People's Republic of China*
[7]*China Center of Advanced Science and Technology, Beijing 100190, People's Republic of China*
[8]*COMSATS University Islamabad, Lahore Campus, Defence Road,*
Off Raiwind Road, 54000 Lahore, Pakistan
[9]*Fudan University, Shanghai 200433, People's Republic of China*
[10]*G.I. Budker Institute of Nuclear Physics SB RAS (BINP), Novosibirsk 630090, Russia*
[11]*GSI Helmholtzcentre for Heavy Ion Research GmbH, D-64291 Darmstadt, Germany*
[12]*Guangxi Normal University, Guilin 541004, People's Republic of China*
[13]*Hangzhou Normal University, Hangzhou 310036, People's Republic of China*
[14]*Helmholtz Institute Mainz, Staudinger Weg 18, D-55099 Mainz, Germany*
[15]*Henan Normal University, Xinxiang 453007, People's Republic of China*
[16]*Henan University of Science and Technology, Luoyang 471003, People's Republic of China*
[17]*Henan University of Technology, Zhengzhou 450001, People's Republic of China*
[18]*Huangshan College, Huangshan 245000, People's Republic of China*
[19]*Hunan Normal University, Changsha 410081, People's Republic of China*
[20]*Hunan University, Changsha 410082, People's Republic of China*
[21]*Indian Institute of Technology Madras, Chennai 600036, India*
[22]*Indiana University, Bloomington, Indiana 47405, USA*
[23a]*INFN Laboratori Nazionali di Frascati, I-00044 Frascati, Italy*
[23a]*INFN Sezione di Perugia, I-06100, Perugia, Italy*
[23a]*University of Perugia, I-06100 Perugia, Italy*
[24a]*INFN Sezione di Ferrara, I-44122 Ferrara, Italy*
[24b]*University of Ferrara, I-44122 Ferrara, Italy*
[25]*Institute of Modern Physics, Lanzhou 730000, People's Republic of China*
[26]*Institute of Physics and Technology, Peace Ave. 54B, Ulaanbaatar 13330, Mongolia*
[27]*Jilin University, Changchun 130012, People's Republic of China*
[28]*Johannes Gutenberg University of Mainz, Johann-Joachim-Becher-Weg 45, D-55099 Mainz, Germany*
[29]*Joint Institute for Nuclear Research, 141980 Dubna, Moscow region, Russia*
[30]*Justus-Liebig-Universitaet Giessen, II. Physikalisches Institut,*
Heinrich-Buff-Ring 16, D-35392 Giessen, Germany
[31]*Lanzhou University, Lanzhou 730000, People's Republic of China*
[32]*Liaoning Normal University, Dalian 116029, People's Republic of China*
[33]*Liaoning University, Shenyang 110036, People's Republic of China*
[34]*Nanjing Normal University, Nanjing 210023, People's Republic of China*
[35]*Nanjing University, Nanjing 210093, People's Republic of China*
[36]*Nankai University, Tianjin 300071, People's Republic of China*
[37]*National Centre for Nuclear Research, Warsaw 02-093, Poland*
[38]*North China Electric Power University, Beijing 102206, People's Republic of China*
[39]*Peking University, Beijing 100871, People's Republic of China*

^{40}Qufu Normal University, Qufu 273165, People's Republic of China
^{41}Shandong Normal University, Jinan 250014, People's Republic of China
^{42}Shandong University, Jinan 250100, People's Republic of China
^{43}Shanghai Jiao Tong University, Shanghai 200240, People's Republic of China
^{44}Shanxi Normal University, Linfen 041004, People's Republic of China
^{45}Shanxi University, Taiyuan 030006, People's Republic of China
^{46}Sichuan University, Chengdu 610064, People's Republic of China
^{47}Soochow University, Suzhou 215006, People's Republic of China
^{48}South China Normal University, Guangzhou 510006, People's Republic of China
^{49}Southeast University, Nanjing 211100, People's Republic of China
^{50}State Key Laboratory of Particle Detection and Electronics,
Beijing 100049, Hefei 230026, People's Republic of China
^{51}Sun Yat-Sen University, Guangzhou 510275, People's Republic of China
^{52}Suranaree University of Technology, University Avenue 111, Nakhon Ratchasima 30000, Thailand
^{53}Tsinghua University, Beijing 100084, People's Republic of China
^{54a}Turkish Accelerator Center Particle Factory Group, Istinye University, 34010, Istanbul, Turkey
^{54b}Near East University, Nicosia, North Cyprus, Mersin 10, Turkey
^{55}University of Chinese Academy of Sciences, Beijing 100049, People's Republic of China
^{56}University of Groningen, NL-9747 AA Groningen, The Netherlands
^{57}University of Hawaii, Honolulu, Hawaii 96822, USA
^{58}University of Jinan, Jinan 250022, People's Republic of China
^{59}University of Manchester, Oxford Road, Manchester M13 9PL, United Kingdom
^{60}University of Minnesota, Minneapolis, Minnesota 55455, USA
^{61}University of Muenster, Wilhelm-Klemm-Str. 9, 48149 Muenster, Germany
^{62}University of Oxford, Keble Rd, Oxford OX13RH, United Kingdom
^{63}University of Science and Technology Liaoning, Anshan 114051, People's Republic of China
^{64}University of Science and Technology of China, Hefei 230026, People's Republic of China
^{65}University of South China, Hengyang 421001, People's Republic of China
^{66}University of the Punjab, Lahore-54590, Pakistan
^{67a}University of Turin and INFN, University of Turin, I-10125 Turin, Italy
^{67b}University of Eastern Piedmont, I-15121 Alessandria, Italy
^{67c}INFN, I-10125 Turin, Italy
^{68}Uppsala University, Box 516, SE-75120 Uppsala, Sweden
^{69}Wuhan University, Wuhan 430072, People's Republic of China
^{70}Xinyang Normal University, Xinyang 464000, People's Republic of China
^{71}Yunnan University, Kunming 650500, People's Republic of China
^{72}Zhejiang University, Hangzhou 310027, People's Republic of China
^{73}Zhengzhou University, Zhengzhou 450001, People's Republic of China

[a]Also at the Moscow Institute of Physics and Technology, Moscow 141700, Russia.
[b]Also at the Novosibirsk State University, Novosibirsk 630090, Russia.
[c]Also at the NRC "Kurchatov Institute", PNPI, 188300 Gatchina, Russia.
[d]Currently at Istanbul Arel University, 34295 Istanbul, Turkey.
[e]Also at Goethe University Frankfurt, 60323 Frankfurt am Main, Germany.
[f]Also at Key Laboratory for Particle Physics, Astrophysics and Cosmology, Ministry of Education; Shanghai Key Laboratory for Particle Physics and Cosmology; Institute of Nuclear and Particle Physics, Shanghai 200240, People's Republic of China.
[g]Also at Key Laboratory of Nuclear Physics and Ion-beam Application (MOE) and Institute of Modern Physics, Fudan University, Shanghai 200443, People's Republic of China.
[h]Also at State Key Laboratory of Nuclear Physics and Technology, Peking University, Beijing 100871, People's Republic of China.
[i]Also at School of Physics and Electronics, Hunan University, Changsha 410082, China.
[j]Also at Guangdong Provincial Key Laboratory of Nuclear Science, Institute of Quantum Matter, South China Normal University, Guangzhou 510006, China.
[k]Also at Frontiers Science Center for Rare Isotopes, Lanzhou University, Lanzhou 730000, People's Republic of China.
[l]Also at Lanzhou Center for Theoretical Physics, Lanzhou University, Lanzhou 730000, People's Republic of China.
[m]Also at the Department of Mathematical Sciences, IBA, Karachi, Pakistan.

Based on a data sample of $(448.1 \pm 2.9) \times 10^6$ $\psi(3686)$ events collected with the BESIII detector at the BEPCII collider, the branching fraction of $\psi(3686) \to \Lambda\bar{\Lambda}\omega$ is measured to be $(3.30 \pm 0.34(\text{stat}) \pm 0.29(\text{syst})) \times 10^{-5}$ for the first time. In addition, the $\Lambda\omega$ (or $\bar{\Lambda}\omega$) invariant mass spectra is studied and the potential presence of excited Λ states has been investigated.

I. INTRODUCTION

Quantum chromodynamics (QCD), the theory which describes the strong interaction, has been tested thoroughly at high energy. However, in the medium energy region, theoretical calculations based on first principles are still unreliable, since nonperturbative contributions are significant and calculations have to rely on models. Experimental measurements in this energy region are helpful to validate models, constrain parameters, and inspire new calculations. Charmonium states are on the boundary between the perturbative and nonperturbative regimes; therefore, their decays, especially hadronic decays, provide ideal inputs to the study of QCD. The availability of very large data samples of vector charmonia, such as J/ψ and $\psi(3686)$, produced via electron-positron annihilations, makes possible experimental studies of rare processes and decay channels with complicated intermediate structures [1].

Among these hadronic decays, scenarios of $\psi(3686)$ and J/ψ decaying into baryon pairs have been understood in terms of $c\bar{c}$ annihilations into three gluons or into a virtual photon [2]. Three-body decays, namely $\psi(3686) \to \Lambda\bar{\Lambda}P$, where P represents a meson such as π^0, η, or ω, are of great interest since intermediate states contribute significantly [3]. Recent studies have focused mainly on the final states $\Lambda\bar{\Lambda}\pi^0$ and $\Lambda\bar{\Lambda}\eta$, and not so much on $\Lambda\bar{\Lambda}\omega$. This is probably due to the fact that the final states $\Lambda\bar{\Lambda}\pi^0$ and $\Lambda\bar{\Lambda}\eta$ allow a test of the "12% rule" [1]. However, it is not possible for $\Lambda\bar{\Lambda}\omega$, since it is heavily suppressed due to the small phase space for the decay of J/ψ to $\Lambda\bar{\Lambda}\omega$. In addition, as the excitation spectra of most hyperons are still not well understood [4], the process $\psi(3686) \to \Lambda\bar{\Lambda}\omega$ provides a good opportunity to search for potential Λ excitations. Multichannel analysis of the quasi-two-body excited hyperon states has been performed in the past; a pole and Breit-Wigner resonance parameters, assigned to $\Lambda(2070) \to \Lambda\omega$ are given as $M = 2044 \pm 20$ MeV/c^2, $\Gamma = 360 \pm 45$ MeV and $M = 2070 \pm 24$ MeV/c^2, $\Gamma = 370 \pm 50$ MeV, respectively [4].

Using the large sample of $(448.1 \pm 2.9) \times 10^6$ $\psi(3686)$ events collected with the BESIII detector, we present the first observation of $\psi(3686) \to \Lambda\bar{\Lambda}\omega$ and the corresponding upper limit of the branching fraction of $\mathcal{B}(\psi(3686) \to \Lambda\bar{\Lambda}^* + \text{c.c.} \to \Lambda\bar{\Lambda}\omega)$.

II. DETECTOR AND DATA SAMPLES

The BESIII detector [5] records symmetric e^+e^- collisions provided by the BEPCII storage ring [6], which operates with a peak luminosity of 1×10^{33} cm^{-2} s^{-1} in the center-of-mass (CM) energy range from 2.0 to 4.9 GeV. BESIII has collected large data samples in this energy region [7]. The cylindrical core of the BESIII detector covers 93% of the full solid angle and consists of a helium-based multilayer drift chamber (MDC), a plastic scintillator time-of-flight (TOF) system, and a CsI(Tl) electromagnetic calorimeter (EMC), which are all enclosed in a superconducting solenoidal magnet providing a 1.0 T magnetic field. The solenoid is supported by an octagonal flux-return yoke with resistive plate counter muon identification modules interleaved with steel. The charged-particle momentum resolution at 1 GeV/c is 0.5%, and the specific energy loss (dE/dx) resolution is 6% for electrons from Bhabha scattering. The EMC measures photon energies with a resolution of 2.5% (5%) at 1 GeV in the barrel (end cap) region. The time resolution in the TOF barrel region is 68 ps, while that in the end cap region is 110 ps.

Simulated data samples produced with GEANT4-based [8] Monte Carlo (MC) software, which includes the geometric description of the BESIII detector and the detector response, are used to optimize the selection criteria, determine detection efficiencies and to estimate backgrounds. The simulation models the beam energy spread and initial state radiation (ISR) in the e^+e^- annihilations with the generator KKMC [9,10]. The inclusive MC simulation includes the production of the $\psi(3686)$ resonance, the ISR production of the J/ψ, and the continuum processes incorporated in KKMC. The known decay modes are modeled with EVTGEN [11,12] using branching fractions taken from the Particle Data Group [13], and the remaining unknown charmonium decays are modeled with LUNDCHARM [14,15]. Final state radiation (FSR) from charged final-state particles is incorporated using PHOTOS [16]. An exclusive phase space MC is used to simulate the $\psi(3686) \to \Lambda\bar{\Lambda}\omega$ reaction. The data sets collected at the CM energies of 3.650 GeV and 3.773 GeV, with an integrated luminosity of $(44.49 \pm 0.02 \pm 0.44)$ pb^{-1} and (2917 ± 29) pb^{-1} [17], respectively, are used to estimate the contamination from the continuum processes of $e^+e^- \to \Lambda\bar{\Lambda}\omega$.

III. EVENT SELECTION AND BACKGROUND ANALYSIS

The process $\psi(3686) \to \Lambda\bar{\Lambda}\omega$ is reconstructed with $\Lambda \to p\pi^-$, $\bar{\Lambda} \to \bar{p}\pi^+$, $\omega \to \pi^+\pi^-\pi^0$ and $\pi^0 \to \gamma\gamma$. The signal events are required to have at least six charged tracks and at least two photon candidates. Charged tracks detected in the MDC are required to be within a polar angle (θ) range of $|\cos\theta| < 0.93$, where θ is defined with respect to the z-axis, which is the symmetry axis of the MDC. A secondary vertex fit is performed for each pair of oppositely charged tracks, and the combinations with χ^2 less than 50 are saved as Λ or $\bar{\Lambda}$ candidates, without further requirements on the decay length. At least one $\Lambda\bar{\Lambda}$ pair is required in each signal event. Particle identification (PID) based on TOF and dE/dx information is applied to the pairs of charged tracks belonging to the Λ ($\bar{\Lambda}$) candidate. The track in the pair with the largest probability calculated under the proton (antiproton) assumption is assumed to be a proton (antiproton), and the other track is assumed to be a pion. If more than one $\Lambda\bar{\Lambda}$ pair survive, the one with the minimum value of $((M_{p\pi^-} - m_\Lambda)^2 + (M_{\bar{p}\pi^+} - m_{\bar{\Lambda}})^2)$ is kept for further analysis, where $M_{p\pi^-}$ ($M_{\bar{p}\pi^+}$) is the invariant mass of $p\pi^-(\bar{p}\pi^+)$ and m_Λ ($m_{\bar{\Lambda}}$) is the known mass of Λ ($\bar{\Lambda}$) [13]. The charged tracks which are not used in the $\Lambda\bar{\Lambda}$ pairs are assumed to originate from ω decays. For these tracks, the distance of closest approach to the e^+e^- interaction point must be less than 10 cm in the z direction, and less than 1 cm in the plane perpendicular to the z direction. They are identified as π if the pion PID likelihood is the largest among the three assumptions of π, K and p. Signal events are selected when at least one pair of $\pi^+\pi^-$ is identified.

Photon candidates are identified using showers in the EMC. The deposited energy of each shower must be greater than 25 MeV in the barrel region ($|\cos\theta| < 0.80$) and greater than 50 MeV in the end cap region ($0.86 < |\cos\theta| < 0.92$). To exclude showers originating from charged particles, the angle between the position of the shower in the EMC and the closest point of the extrapolated trajectory of each charged track must be greater than 10 degrees; because of the large number of secondary photons produced in antiproton annihilations [18], the angle between the position of the shower and the extrapolated trajectory point of antiproton tracks must be greater than 30 degrees. To suppress electronic noise and showers unrelated to the event, the difference between the EMC time and the event start time is required to be within (0, 700) ns. The π^0 candidates are reconstructed through $\pi^0 \to \gamma\gamma$ decays, and a kinematic fit that constrains the invariant mass to the π^0 known mass is performed [13]. The χ^2 of the kinematic fit is required to be less than 25.

To improve the mass resolution, a five-constraint (5C) kinematic fit for the $\psi(3686) \to \Lambda\bar{\Lambda}\pi^+\pi^-\gamma\gamma$ hypothesis is performed, where in addition to energy-momentum

conservation, the invariant mass of the two photons is constrained to the known mass of π^0. Figure 1(a) shows the χ^2 of the 5C fit, which is required to be less than 40. For events with more than one combination satisfying this requirement, the combination with the smallest χ^2 is kept.

For the surviving events, $\Lambda(\bar{\Lambda})$ candidates are selected by requiring $|M_{p\pi^-(\bar{p}\pi^+)} - m_{\Lambda(\bar{\Lambda})}| < 5 \text{ MeV}/c^2$, as shown in Figs. 1(b) and 1(c). Backgrounds from $\psi(3686) \to \pi^+\pi^- J/\psi$ decays are rejected by requiring $|M^{\text{rec}}_{\pi^+\pi^-} - m_{J/\psi}| > 30 \text{ MeV}/c^2$, where $M^{\text{rec}}_{\pi^+\pi^-}$ is the recoil mass of the $\pi^+\pi^-$ system decaying from ω and $m_{J/\psi}$ is the known mass of J/ψ [13], as shown in Fig. 1(d).

To study the background contributions, the same selection criteria are applied to the $\psi(3686)$ inclusive MC simulation. A topological analysis of the events surviving to the selections has been performed with TopoAna [19], and the number of background events with ω in the final state is negligible. Therefore, the background contributions are estimated using the ω sideband events from data, where the sideband regions are defined as $0.693 \text{ GeV}/c^2 < M_{\pi^+\pi^-\pi^0} < 0.723 \text{ GeV}/c^2$ and $0.843 \text{ GeV}/c^2 < M_{\pi^+\pi^-\pi^0} < 0.873 \text{ GeV}/c^2$, and the signal region as $0.753 \text{ GeV}/c^2 < M_{\pi^+\pi^-\pi^0} < 0.813 \text{ GeV}/c^2$. To investigate the amount of possible background from continuum processes, the same selection criteria are applied to data samples of $(2917 \pm 29) \text{ pb}^{-1}$ collected at $\sqrt{s} = 3.773 \text{ GeV}$ and $(44.49 \pm 0.02 \pm 0.44) \text{ pb}^{-1}$ collected at $\sqrt{s} = 3.650 \text{ GeV}$ [17], and no event survives after applying all the selection criteria [20]. Hence, background from the continuum contribution of the electromagnetic process $e^+e^- \to \Lambda\bar{\Lambda}\omega$ is negligible.

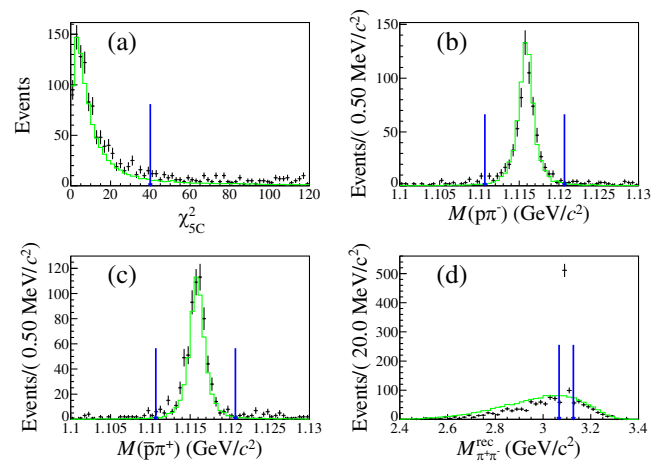FIG. 1.   (a) The χ^2 distribution of the 5C fit, (b) the invariant mass distribution of $p\pi^-$ and (c) $\bar{p}\pi^+$, and (d) the recoil mass of the $\pi^+\pi^-$ system from the decaying ω. Dots with error bars are $\psi(3686)$ data, and the green histograms show the phase space MC simulation of $\psi(3686) \to \Lambda\bar{\Lambda}\omega$. The blue arrows show the applied selections. The simulation is normalized to the maximum bin value of the data in (a),(b) and (c), and to the data integral in (d).

IV. BRANCHING FRACTION MEASUREMENT OF $\psi(3686) \to \Lambda\bar{\Lambda}\omega$

An unbinned maximum likelihood fit is performed to the invariant mass distribution of $\pi^+\pi^-\pi^0$, as shown in Fig. 2, to determine the number of ω signal events. The ω signal shape is taken from signal MC simulation, and the background is described by a first order Chebyshev polynomial. The branching fraction (BF) of $\psi(3686) \to \Lambda\bar{\Lambda}\omega$ is calculated according to

$$\mathcal{B}(\psi(3686) \to \Lambda\bar{\Lambda}\omega) = \frac{N_{obs}}{N_{\psi(3686)} \cdot \mathcal{B} \cdot \varepsilon}, \quad (1)$$

where $N_{obs} = 207 \pm 21$ is the number of ω signal events obtained from the fit, $\varepsilon = (3.89 \pm 0.02)\%$ is the detection efficiency, estimated from $\psi(3686) \to \Lambda\bar{\Lambda}\omega$ MC simulation, and $\mathcal{B}$ is the product of branching ratios of $\mathcal{B}(\Lambda \to p\pi^-) \cdot \mathcal{B}(\bar{\Lambda} \to \bar{p}\pi^+) \cdot \mathcal{B}(\omega \to \pi^+\pi^-\pi^0) \cdot \mathcal{B}(\pi^0 \to \gamma\gamma)$ [13]. $\mathcal{B}(\psi(3686) \to \Lambda\bar{\Lambda}\omega)$ is measured to be $(3.30 \pm 0.34(\text{stat})) \times 10^{-5}$, where the uncertainty is statistical only.

V. STUDY OF INTERMEDIATE STATES

In order to study possible intermediate states in $\psi(3686) \to \Lambda\bar{\Lambda}\omega$, an additional requirement of $|M_{\pi^+\pi^-\pi^0} - m_\omega| < 30 \text{ MeV}/c^2$ is applied, where m_ω is the mass of the ω meson [13]. The Dalitz plot of $M^2(\bar{\Lambda}\omega)$ versus $M^2(\Lambda\omega)$ is shown in Fig. 3. A two-dimensional unbinned maximum likelihood fit is performed to the Dalitz plot to investigate the potential exited Lambda state Λ^*, which could decay as $\Lambda^* \to \Lambda\omega(\overline{\Lambda^*} \to \bar{\Lambda}\omega)$. In the fit, the signal of Λ^* is modeled with an S-wave Breit-Wigner function in two dimensions [21], namely,
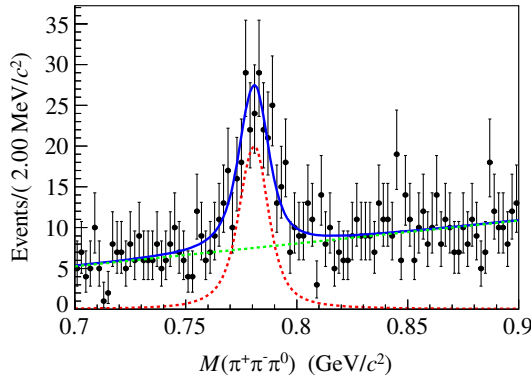

FIG. 2. Invariant mass spectrum of the $\pi^+\pi^-\pi^0$ system. Dots with error bars are data, and the blue solid curve shows the fit result. The red dashed curve is the ω signal shape, and the green dashed curve is the background.
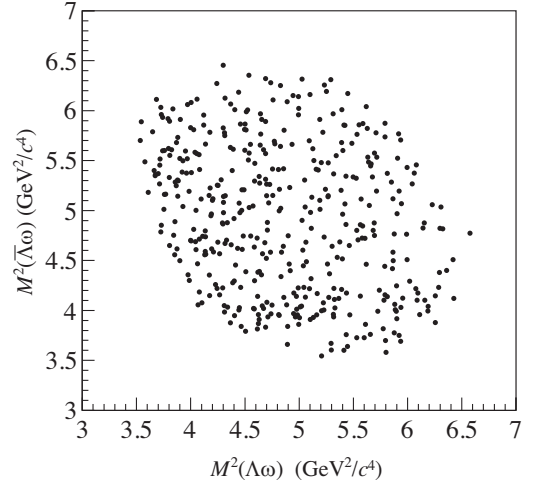

FIG. 3. Dalitz plot of $M^2(\bar{\Lambda}\omega)$ versus $M^2(\Lambda\omega)$ from data.

$$\epsilon(x,y) \cdot \left(\frac{p \cdot q}{(M_R^2 - x)^2 + M_R^2 \cdot \Gamma^2} \right.$$
$$\left. + \frac{p \cdot q}{(M_R^2 - y)^2 + M_R^2 \cdot \Gamma^2} \right) \otimes \sigma(x,y), \quad (2)$$

where x and y correspond to $M^2(\Lambda\omega)$ and $M^2(\bar{\Lambda}\omega)$, respectively; M_R and Γ are the mass and width of $\Lambda^*/\bar{\Lambda}^*$; p is the momentum of $\Lambda^*/\bar{\Lambda}^*$ in the c.m. frame; q is the momentum of ω in the rest frame of $\Lambda^*/\bar{\Lambda}^*$; $\sigma(x,y)$, is the two dimensional Gaussian resolution function, obtained from a zero width Λ^* and $\bar{\Lambda}^*$ signal MC simulation, and $\epsilon(x,y)$ is the two dimensional detection efficiency function of x and y, which is obtained from $\psi(3686) \to \Lambda\bar{\Lambda}\omega$ exclusive MC simulation. Due to the low statistics, possible interference effects are not considered in the analysis. The probability density function of the process $\psi(3686) \to \Lambda\bar{\Lambda}\omega$ without intermediate states is taken from MC simulation. The non $-\omega$ background is described by the normalized ω sidebands.

The fit projections of $M^2(\Lambda\omega)$ and $M^2(\bar{\Lambda}\omega)$ are shown in Fig. 4. From the fit, 51 ± 16 signals are obtained, with statistical significance of 3.1σ, which is evaluated by comparing the likelihood values with and without the Λ^* resonance included in the fit. To take into account the additive systematic uncertainties related to the fits, alternative fits with different ω sideband background levels and shapes are performed, and the minimum significance among these cases is 3.0σ. The fitted $\Lambda^*/\bar{\Lambda}^*$ mass and width are $M_{\Lambda^*/\bar{\Lambda}^*} = 2.001 \pm 0.007 \text{ GeV}/c^2$ and $\Gamma_{\Lambda^*/\bar{\Lambda}^*} = 0.036 \pm 0.014 \text{ GeV}/c^2$. If compared with the excited states with similar mass listed in the Review of Particle Properties [13], like $\Lambda(2000)$, $\Lambda(2050)$ and $\Lambda(2070)$, the fitted width of $36 \text{ MeV}/c^2$ is below the reported value of these states, which is between 100 and 400 MeV/c^2. It is evident that higher statistics and a detailed partial wave analysis are
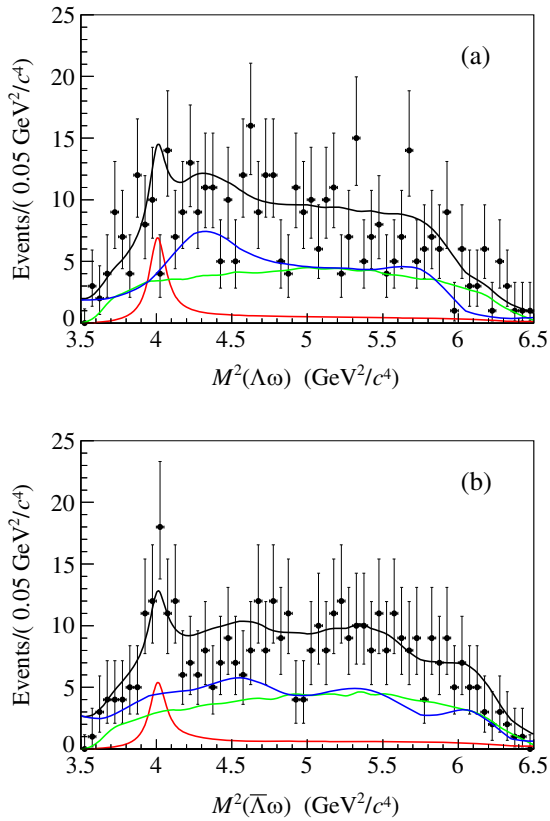
FIG. 4. The distributions of (a) $M^2(\Lambda\omega)$ (b) and $M^2(\bar{\Lambda}\omega)$. Dots with error bars are data, the black solid curves are projections from the fits, the red solid curves show the shape of $\Lambda^*/\bar{\Lambda}^*$ resonances, the blue solid curves show the background described by ω sidebands and the green solid curves show the shapes from the nonresonant decay $\psi(3686) \to \Lambda\bar{\Lambda}\omega$. The $\Lambda\omega$ and $\bar{\Lambda}\omega$ invariant masses are fitted simultaneously giving the same yield for the $\Lambda\omega$ and $\bar{\Lambda}\omega$ excited state. The differences between the $\Lambda\omega$ and $\bar{\Lambda}\omega$ invariant masses in the fitted curves in (a) and (b) for the signal and the background are due to different detection efficiencies of $\Lambda\omega$ and $\bar{\Lambda}\omega$.

needed in order to decide whether this structure is present and if its properties are consistent with one of these states or not.

The BF of $\psi(3686) \to \Lambda\bar{\Lambda}^* + \text{c.c.} \to \Lambda\bar{\Lambda}\omega$ according to

$$\mathcal{B}(\psi(3686) \to \Lambda\bar{\Lambda}^* + \text{c.c.} \to \Lambda\bar{\Lambda}\omega) = \frac{N_{\text{sig}}}{N_{\psi(3686)} \cdot \mathcal{B} \cdot \epsilon}$$

$$= (8.91 \pm 2.82(\text{stat}) \pm 0.73(\text{sys.})) \times 10^{-6}, \quad (3)$$

where $N_{\text{sig}} = 51 \pm 16$ is the number of Λ^* signal events obtained from the fit, $\epsilon = (3.59 \pm 0.02)\%$ is the detection efficiency, estimated from $\psi(3686) \to \Lambda\bar{\Lambda}^* + \text{c.c.} \to \Lambda\bar{\Lambda}\omega$ MC simulation and $\mathcal{B}$ is the product of branching ratios as Eq. (3). Since only a few signal events are observed and the significance is only 3σ, to be conservative, the branching fraction upper limit of $\psi(3686) \to \Lambda\bar{\Lambda}^* + \text{c.c.} \to \Lambda\bar{\Lambda}\omega$ is

measured. The upper limit on the number of signal events, $N_{\text{sig}}^{\text{up}}$, is determined at the 90% confidence level (CL) by solving [22]

$$\int_0^{N_{\text{sig}}^{\text{up}}} \mathcal{L}(\mu)d\mu \Big/ \int_0^{+\infty} \mathcal{L}(\mu)d\mu = 0.9, \quad (4)$$

where μ is the number of fitted signal events, and $\mathcal{L}(\mu)$ is the likelihood function obtained from the fit to data. To determine the upper limit on the Λ^* resonance signal events, a series of unbinned maximum-likelihood fits are performed to the Dalitz plot of $M^2(\bar{\Lambda}\omega)$ versus $M^2(\Lambda\omega)$ with a varying number of expected Λ^* resonance signal events. To take into account the additive systematic uncertainties related to the fits, alternative fits with different ω sideband background levels and shapes are performed, and the maximum upper limit among these cases is determined. To account for the multiplicative systematic uncertainties, the likelihood distribution is convolved with a Gaussian function $G(x; 0, \sigma)$ with a standard deviation of $\sigma = x \times \Delta$ [22],

$$\mathcal{L}'(\mu) = \int_0^{+\infty} \mathcal{L}(x) \times G(\mu - x; 0, \sigma)dx \quad (5)$$

where μ is the expected number of signal events, $\mathcal{L}'(\mu)$ indicates the expected likelihood distribution, and Δ refers to the total relative systematic uncertainty listed in Table I.

The branching fraction upper limit of $\psi(3686) \to \Lambda\bar{\Lambda}^* + \text{c.c.} \to \Lambda\bar{\Lambda}\omega$ is calculated as follows:

$$\mathcal{B}(\psi(3686) \to \Lambda\bar{\Lambda}^* + \text{c.c.} \to \Lambda\bar{\Lambda}\omega) < \frac{N_{\text{sig}}^{\text{up}}}{N_{\psi(3686)} \cdot \mathcal{B} \cdot \epsilon}, \quad (6)$$

where $N_{\text{sig}}^{\text{up}}$ is the upper limit of the number of signal events, $\epsilon = (3.59 \pm 0.02)\%$ is the detection efficiency, estimated from $\psi(3686) \to \Lambda\bar{\Lambda}^* + \text{c.c.} \to \Lambda\bar{\Lambda}\omega$ MC simulation, and $\mathcal{B}$ is the product of branching ratios of $\mathcal{B}(\Lambda \to p\pi^-) \cdot \mathcal{B}(\bar{\Lambda} \to \bar{p}\pi^+) \cdot \mathcal{B}(\omega \to \pi^+\pi^-\pi^0) \cdot \mathcal{B}(\pi^0 \to \gamma\gamma)$ [13]. The red and black solid curves in Fig. 5 show the updated and the raw likelihood distributions, respectively. The upper limit of the number of signal events is 80.1, and the upper limit of the branching fraction is 14×10^{-6} at the 90% CL.

VI. SYSTEMATIC UNCERTAINTIES

The sources of systematic uncertainties are summarized in Table I. The second and third columns present the uncertainties for the branching fraction measurement of $\psi(3686) \to \Lambda\bar{\Lambda}\omega$ and the upper limit of $\mathcal{B}(\psi(3686) \to \Lambda\bar{\Lambda}^* + \text{c.c.} \to \Lambda\bar{\Lambda}\omega)$, respectively.

Number of $\psi(3686)$ events: The uncertainty due to the number of $\psi(3686)$ events is 0.7% [23].

Tracking efficiency; The uncertainty due to data-MC difference in the tracking efficiency is 1.0% for each

TABLE I.   Systematic uncertainties in %.

Source		$\psi(3686) \to \Lambda\bar{\Lambda}\omega$	Upper limit of $\Lambda^*/\bar{\Lambda}^*$
Number of $\psi(3686)$ events		0.7	0.7
MDC tracking		6.0	6.0
PID efficiency		4.0	4.0
Photon detection efficiency		2.0	2.0
$\Lambda\bar{\Lambda}$ reconstruction efficiency		2.0	2.0
Kinematic fit		1.5	1.5
Intermediate decay	$\Lambda \to p\pi^-$	0.8	0.8
	$\bar{\Lambda} \to \bar{p}\pi^+$	0.8	0.8
	$\omega \to \pi^+\pi^-\pi^0$	0.7	0.7
	$\pi^0 \to \gamma\gamma$	0.03	0.03
Mass window	Λ	0.02	0.04
	$\bar{\Lambda}$	0.03	0.02
	J/ψ	1.6	1.8
	ω	$\cdots$	0.02
Fitting	Signal shape	2.9	$\cdots$
	Background shape	1.4	$\cdots$
	Fit range	1.5	$\cdots$
Total		8.9	8.2

charged track coming from a primary vertex, according to a study based on $J/\psi \to K^*\bar{K}$ and $J/\psi \to p\bar{p}\pi^+\pi^-$ events [24]. For tracks coming from $\Lambda(\bar{\Lambda})$ decays, the uncertainty is also 1.0%, estimated by an analysis of $J/\psi \to \bar{p}K^+\Lambda$ events [24].

PID efficiency: In this analysis, the particle identification is applied to the $p(\bar{p})$ from $\Lambda(\bar{\Lambda})$ decays, and to the π^+ and π^- from ω decays. The PID efficiency has been investigated using control samples of $J/\psi \to K_S^0 K^\pm \pi^\pm$ and $J/\psi \to p\bar{p}\pi^+\pi^-$ [25,26]. The uncertainty is assigned to be 1.0% per charged track; thus the total systematic uncertainty is 4.0%.
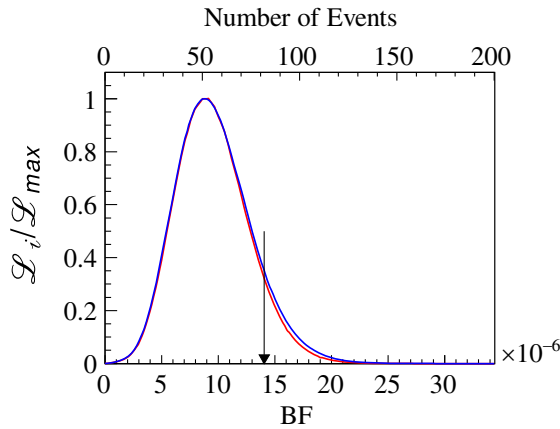
FIG. 5.   Distribution of likelihood versus number of signal events (and BF) for data. The results obtained with and without incorporating the systematic uncertainties are shown in blue solid and red solid curves, respectively. The black arrow shows the results corresponding to the 90% CL.

Photon detection efficiency: The uncertainty in the photon reconstruction is studied by using the control sample $\psi(3686) \to \pi^+\pi^- J/\psi$, $J/\psi \to \rho^0\pi^0$, and a 1.0% systematic uncertainty is estimated for each photon [25].

$\Lambda\bar{\Lambda}$ *reconstruction efficiency*: The uncertainties due to the Λ and $\bar{\Lambda}$ secondary vertex fits are determined to be 1.0% each, as presented in Ref. [3]. In this work, a 2.0% systematic uncertainty is estimated for the $\Lambda\bar{\Lambda}$ reconstruction efficiency.

Kinematic fit: The systematic uncertainty due to kinematic fitting is estimated by correcting the helix parameters of charged tracks according to the method described in Ref. [27]. The difference between the detection efficiencies with and without this correction is considered as the systematic uncertainty, which is 1.5%. The detection efficiencies with this correction is nominal result.

Intermediate decays: The systematic uncertainties on the intermediate-decays $\Lambda \to p\pi^-$, $\bar{\Lambda} \to \bar{p}\pi^+$, $\omega \to \pi^+\pi^-\pi^0$ and $\pi^0 \to \gamma\gamma$ are from the PDG [13].

Mass window: The systematic uncertainty from the requirement on the $\Lambda(\bar{\Lambda}, \omega)$ signal region is estimated by smearing the $p\pi^-(\bar{p}\pi^+, \pi^+\pi^-\pi^0)$ invariant mass in the signal MC simulation with a Gaussian function to compensate for the resolution difference between data and MC simulation. The smearing parameters are determined by fitting the $p\pi^-(\bar{p}\pi^+, \pi^+\pi^-\pi^0)$ invariant mass distribution in data with the MC-simulated shape convolved with a Gaussian function. The difference in the detection efficiency as determined from the signal MC simulation with and without the extra smearing is taken as the systematic uncertainty. The systematic uncertainties related to the vetoed J/ψ mass window are estimated by

varying the size of the mass window, i.e., contracting/expanding it by $2\,\text{MeV}/c^2$. The resulting differences of branching fractions are treated as the systematic uncertainties.

Fit range: To estimate the systematic uncertainty due to the fit range, several alternative fits in different ranges ($[0.69, 0.89]\,\text{GeV}/c^2$, $[0.71, 0.91]\,\text{GeV}/c^2$, $[0.69, 0.91]\,\text{GeV}/c^2$ and $[0.71, 0.89]\,\text{GeV}/c^2$) are performed. The largest resulting difference in the BF is assigned as the systematic uncertainty.

Signal shape: To estimate the uncertainty due to the choice of the signal shape, the MC-simulated shape is replaced by MC-simulated shape convolved with a Gaussian function, and the resulting differences in the BFs are assigned as systematic uncertainties.

Background shape: To estimate the systematic uncertainty due to choice of the background shape, an alternative fit is performed by replacing the first order Chebyshev polynomial with a second-order Chebyshev polynomial. The change in the measured BF is assigned as the corresponding systematic uncertainty.

The total systematic uncertainty is calculated by assuming the individual components to be independent, and adding their magnitudes in quadrature.

VII. SUMMARY

The process $\psi(3686) \to \Lambda\bar{\Lambda}\omega$ is observed for the first time, using $(448.1 \pm 2.9) \times 10^6 \, \psi(3686)$ events collected with the BESIII detector. The branching fraction $\mathcal{B}(\psi(3686) \to \Lambda\bar{\Lambda}\omega)$ is measured to be $(3.30 \pm 0.34(\text{stat}) \pm 0.29(\text{syst})) \times 10^{-5}$. In addition, the potential excited Λ states are investigated by an unbinned maximum likelihood fit to the Dalitz plot. The results hint in agreement with a resonant structure with a mass around $2\,\text{GeV}/c^2$, which could be explained as an excited state Λ^*, but its significance (3.0σ) is not sufficient to claim an observation. The corresponding upper limit for the branching fraction $\mathcal{B}(\psi(3686) \to \Lambda\bar{\Lambda}^* + \text{c.c.} \to \Lambda\bar{\Lambda}\omega)$ is determined to be 1.40×10^{-5} at the 90% confidence level.

[1] M. Ablikim *et al.* (BESIII Collaboration), Phys. Rev. D **99,** 032006 (2019).

[2] K. Zhu, X. H. Mo, and C. Z. Yuan, Int. J. Mod. Phys. A **30,** 1550148 (2015).

[3] M. Ablikim *et al.* (BESIII Collaboration), Phys. Rev. D **87,** 052007 (2013).

[4] A. V. Sarantsev, M. Matveev, V. A. Nikonov, A. V. Anisovich, U. Thoma, and E. Klempt, Eur. Phys. J. A **55,** 180 (2019).

[5] M. Ablikim *et al.* (BESIII Collaboration), Nucl. Instrum. Methods Phys. Res., Sect. A **614,** 345 (2010).

[6] C. H. Yu *et al.*, *Proceedings of IPAC2016, Busan, Korea* (JACoW, Busan, 2016).

[7] M. Ablikim *et al.* (BESIII Collaboration), Chin. Phys. C **44,** 040001 (2020).

[8] S. Agostinelli *et al.* (GEANT4 Collaboration), Nucl. Instrum. Methods Phys. Res., Sect. A **506,** 250 (2003).

[9] S. Jadach, B. F. L. Ward, and Z. Was, Phys. Rev. D **63**, 113009 (2001).

[10] S. Jadach, B. F. L. Ward, and Z. Was, Comput. Phys. Commun. **130**, 260 (2000).

[11] D. J. Lange, Nucl. Instrum. Methods Phys. Res., Sect. A **462**, 152 (2001).

[12] R. G. Ping, Chin. Phys. C **32**, 599 (2008).

[13] P. A. Zyla *et al.* (Particle Data Group), Prog. Theor. Exp. Phys. **2020**, 083C01 (2020).

[14] J. C. Chen, G. S. Huang, X. R. Qi, D. H. Zhang, and Y. S. Zhu, Phys. Rev. D **62**, 034003 (2000).

[15] R. L. Yang, R. G. Ping, and H. Chen, Chin. Phys. Lett. **31**, 061301 (2014).

[16] E. Richter-Was, Phys. Lett. B **303**, 163 (1993).

[17] M. Ablikim (BESIII Collaboration), Chin. Phys. C **37**, 123001 (2013).

[18] M. Ablikim *et al.* (BESIII Collaboration), Phys. Lett. B **771**, 45 (2017).

[19] X. Zhou, S. Du, G. Li, and C. Shen, Comput. Phys. Commun. **258**, 107540 (2021).

[20] M. Ablikim *et al.* (BESIII Collaboration), Phys. Rev. D **100**, 052010 (2019).

[21] M. Ablikim *et al.* (BESIII Collaboration), Phys. Rev. D **97**, 052001 (2018).

[22] M. Ablikim *et al.* (BESIII Collaboration), Phys. Rev. D **98**, 032014 (2018).

[23] M. Ablikim *et al.* (BESIII Collaboration), Chin. Phys. C **42**, 023001 (2018).

[24] M. Ablikim *et al.* (BESIII Collaboration), Phys. Rev. D **87**, 012007 (2013).

[25] M. Ablikim *et al.* (BESIII Collaboration), Phys. Rev. D **83**, 112005 (2011).

[26] M. Ablikim *et al.* (BESIII Collaboration), Phys. Rev. D **85**, 092012 (2012).

[27] M. Ablikim *et al.* (BESIII Collaboration), Phys. Rev. D **87**, 012002 (2013).